Energy & Environmental Science

ROYAL SOCIETY OF CHEMISTRY

COMMUNICATION

View Article Online
View Journal | View Issue

Check for updates

Cite this: *Energy Environ. Sci.*, 2020, **13**, 4862

Received 11th September 2020,
Accepted 23rd October 2020

DOI: 10.1039/d0ee02927k

rsc.li/ees

Low energy intensity production of fuel-grade bio-butanol enabled by membrane-based extraction†

Ji Hoon Kim,[a] Marcus Cook,[a] Ludmila Peeva,[a] Jet Yeo,[a] Leslie W. Bolton,[b] Young Moo Lee[c] and Andrew G. Livingston*[ad]

Widespread use of biofuels is inhibited by the significant energy burden of recovering fuel products from aqueous fermentation systems. Here, we describe a membrane-based extraction (perstraction) system for the recovery of fuel-grade biobutanol from fermentation broths which can extract *n*-butanol with high purity (>99.5%) while using less than 25% of the energy of current technology options. This is achieved by combining a spray-coated thin-film composite membrane with 2-ethyl-1-hexanol as an extractant. The membrane successfully protects the micro-organisms from the extractant, which, although ideal in other respects, is a metabolic inhibitor. In contrast to water, the extractant does not form a heterogeneous azeotrope with *n*-butanol, and the overall energy consumption of for *n*-butanol production is 3.9 MJ kg^{-1}, substantially less than other recovery processes (17.0–29.4 MJ kg^{-1}). By (a) extracting *n*-butanol from the fermentation broth without a phase change, (b) breaking the heterogeneous azeotrope relationship (less energy consumption for distillation), and (c) utilizing a small volume ratio of extractant : fermentation broth (1 : 100, v/v), the need for high energy intensity processes such as pervaporation, gas stripping or liquid–liquid extraction is avoided. The application of this perstraction system to continuous production of a range of higher alcohols is explored and shown to be highly favourable.

Broader context

The WHO included air pollution and climate change amongst the top 10 threats to global health in 2019. Global efforts are endeavouring to replace fossil fuels with renewable energy sources such as solar, wind, hydrogen, and nuclear power. However, these alternatives are limited by the trade-off between energy footprint *vs.* practical convenience. One major bottleneck is the requirement for energy storage infrastructure to provide stable power transmission. Lithium-ion batteries have the highest energy density amongst the energy storage systems currently available, but even this is typically less than 1 MJ kg^{-1} (theoretical maximum is 2 MJ kg^{-1}),[1] one order of magnitude lower than the energy density of liquid fuels (27–47 MJ kg^{-1}).[2] Therefore, for large-scale applications including transportation, renewable liquid fuels are promising candidates to replace or supplement fossil fuels without any modification to current internal combustion engines and their supporting infrastructure. Their widespread use could reduce carbon footprints by 35–60%, and lead to the fixation of 123 billion metric tons per year of carbon dioxide from atmosphere.[3,4] Herein, we introduce an energy-efficient fuel-grade biobutanol production process with *in situ* butanol recovery to capture biologically produced higher alcohols, reducing the energy burden substantially.

1. Introduction

Biofuels provide a potential route to replacing fossil fuels, and so offer competition to batteries and electric vehicles in the transportation and aviation fields.[1,2] Liquid biofuels derived from biomass have the advantages of: (a) reducing net carbon dioxide and particulate emissions by up to 80%; (b) fixing approximately 123 billion metric tons of CO_2 per year from the atmosphere, and; (c) utilising sustainable resources (1 billion dry tons per year of biomass) that are not currently used to produce biodiesel.[2–4] Although liquid biofuels have great potential to harness chemical energy from biomass and to minimize environmental burdens, their price is currently almost twice that of petroleum fuels. This is partly due to the challenging energy-intensive conversion processes that have low yields at every step (hydrolysis, fermentation, and recovery).[2,5] Nevertheless, bioethanol has been successfully commercialized for usage in transportation and power generation (581 TWh per year in 2018) supported by government policies such as the US Renewable Fuel Standard (RSF2) and

[a] *Barrer Centre, Department of Chemical Engineering, Imperial College London, London, SW7 2AZ, UK. E-mail: a.livingston@imperial.ac.uk*
[b] *BP plc, Chertsey Road, Sunbury-on-Thames, Middlesex TW16 7LN, UK*
[c] *Department of Energy Engineering, Hanyang University, Seoul, 04763, Republic of Korea*
[d] *School of Engineering and Materials Science, Queen Mary University of London, London, E1 4NS, UK*

† Electronic supplementary information (ESI) available: Information on all the details regarding materials, membrane fabrication, perstraction test, fermentation, and theoretical calculation. See DOI: 10.1039/d0ee02927k

Open Access Article. Published on 24 October 2020. Downloaded on 3/12/2021 3:23:00 PM. This article is licensed under a Creative Commons Attribution-NonCommercial 3.0 Unported Licence.

This journal is © The Royal Society of Chemistry 2020

Open Access Article. Published on 24 October 2020. Downloaded on 3/12/2021 3:23:00 PM.
This article is licensed under a Creative Commons Attribution-NonCommercial 3.0 Unported Licence.

EU Renewable Energy Directive (EU RED).[5,6] Both E10 and E85 fuels (10% and 85% by volume ratio ethanol respectively) can currently be found in gas stations globally. The majority of conventional combustion engines can utilise an E10 fuel directly. For higher ethanol concentrations, *e.g.* E85, the vehicle must be manufactured as a Flexible Fuel Vehicle, and equipped with ethanol compatible components to accommodate for the different chemical properties and energy content of this biofuel.[7] Other than these modifications, these FFVs run in a near-identical manner to their petroleum based counterparts.[8] The higher alcohols have attractive properties such as a greater energy density, lower hygroscopic and corrosive properties, inherent lubricity, higher cetane number (shorter ignition delay), lower self-ignition temperature, higher flash point, lower volatility, and higher viscosity, when compared to bioethanol, all of which lead to better atomization and combustion (Table S1, ESI†).[6,9,10] Furthermore, the higher alcohols can be used in blends with petroleum products at a higher proportion than ethanol, or as pure fuels for road transportation and aviation.[5,11] In 2018, airlines worldwide committed to purchasing 6 billion litres of biodiesel for aviation, and the Scandinavian airline (SAS) aims to replace all jet fuels for domestic flights with biofuel by 2030. Furthermore, 13 airlines operating at Seattle-Tacoma International Airport in the United States have agreed to collaborate on a plan to utilise sustainable biofuels.[6]

Notwithstanding these advantages, production of biofuels including higher alcohols faces many challenges to become economically feasible. These include: (a) low yielding processes; (b) toxicity to/inhibition of micro-organisms; and (c) energy-intensive recovery systems. Fig. 1a illustrates the current steps from upstream (production) to downstream (recovery) of higher alcohol production. Upstream, the biomass is converted into fermentable feedstock by acidification.[12] Depending on the types of micro-organisms and engineered metabolisms, various types of higher alcohols (*n*-butanol, iso-butanol, *n*-pentanol, and iso-pentanol) can be produced from the feedstock.[2,9] However, the higher alcohols cannot be produced up to high titre (concentration must be less than 2% for butanol and less than 1% for pentanol) due to the toxicity of the higher alcohols to the micro-organisms.[9,13] To improve efficiency of the processes, genetically modifying the micro-organisms to endure high titre of the produced alcohols, and developing energy-efficient recovery systems, have been investigated.[13,14] Recent engineering approaches targeting energy-efficient recovery have shown significant improvements in productivity and yield of the systems by recovering alcohols during fermentation to promote alcohol production beyond the maximum titre of the micro-organism.[15,16] Recovery of alcohols by distillation can generate fuel-grade material (99.5%), but since the distillation process requires the entire broth to be heated to its boiling point to evaporate the alcohol, it has a high energy consumption (typically 35 MJ kg^{-1} in the case of *n*-butanol).[17,18] This is similar to the energy density of *n*-butanol (33 MJ kg^{-1}). Therefore, more energy-efficient recovery systems are essential.

Two distinct approaches have been investigated: (i) dehydration processes and (ii) extractive recovery. In Fig. 1b, the dehydration processes recover produced alcohol with a condenser through phase change by gas stripping (GS, Fig. 1c) or pervaporation (PV, Fig. 1d). Both GS and PV collect vaporized alcohols together with water vapour in a condenser. Consequently, the final content of alcohol in the condenser does not exceed 50% due to limited selectivity which is a fractional ratio of the product in feed and permeate solution (eqn (S1) and Table S2, ESI†), and subsequent

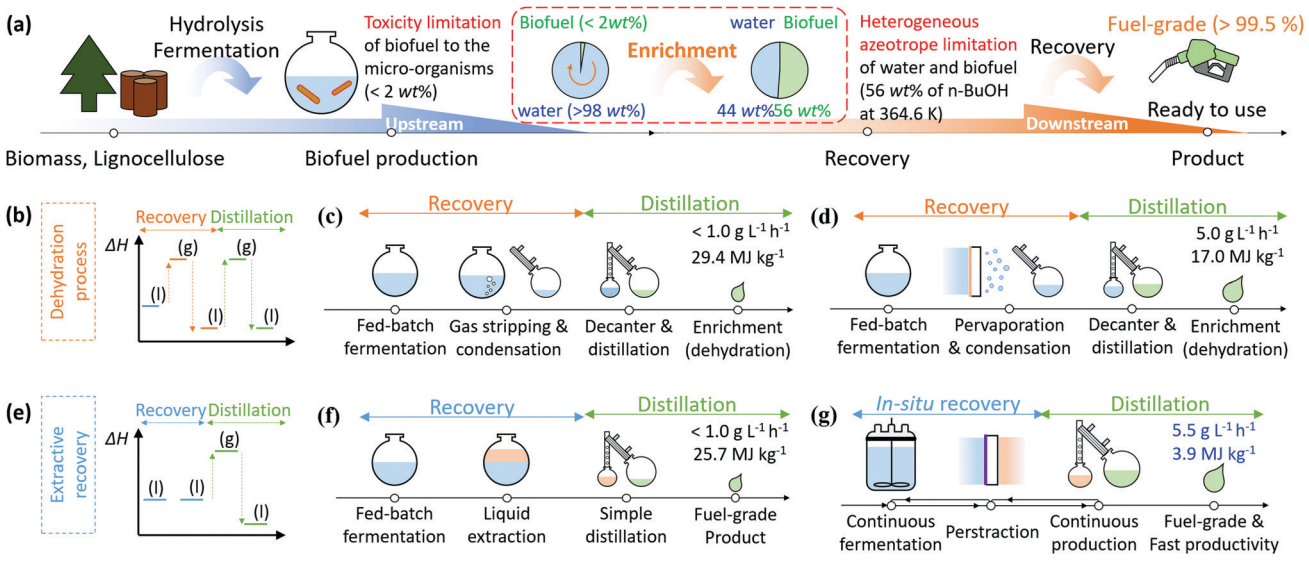


Fig. 1 (a) A schematic diagram of biofuel production process and challenging issues especially for higher alcohols such as butanol and pentanol. (b) Enthalpy diagram showing liquid to gas phase changes of product through dehydration processes including (c) gas stripping (GS) and (d) pervaporation (PV). (e) Enthalpy diagram for phase changes of the product through extractive recovery systems including (f) liquid–liquid extraction (LL) and (g) perstraction (PS, membrane-based extraction). The detailed calculations of productivity and energy consumption are described in Section S1 and Tables S3 and S4 (ESI†).[15–17,19–21]

Open Access Article. Published on 24 October 2020. Downloaded on 3/12/2021 3:23:00 PM.
This article is licensed under a Creative Commons Attribution-NonCommercial 3.0 Unported Licence.

azeotropic distillation requires an additional 17.0–29.4 MJ kg^{-1} (Table S3, ESI†). In contrast, the extractive recovery systems (Fig. 1e) can recover the produced alcohols at high concentration using extraction without phase change. Liquid–liquid extraction (LL, Fig. 1f) is the most common process in liquid biofuel production. The extractant should be non-toxic to micro-organisms, be immiscible with water, and have a high partition coefficient. The partition coefficient (P) is the ratio of concentrations of solute (i) at equilibrium between two immiscible liquids having an interface ($P^{i} = C^{i}_{extractant}/C^{i}_{fermentationbroth}$). Since the extractants typically have extremely low water solubility, the extracted biofuel can be purified to the fuel-grade products through a simple non-azeotropic distillation, and the extractant, which has only limited volatilisation due to higher boiling point than alcohols, is returned to the liquid–liquid process. Unfortunately, extractants with higher partition coefficients are usually toxic to most fermentation organisms, so extractants with low partition coefficients are normally used. Consequently, extractant volumes greater than 50% of the fermentation broth volume are usually required, resulting in relatively high energy consumption (25.7 MJ kg^{-1}, Table S3, ESI†) during distillation of the extracted alcohols. The most common extractant, oleyl alcohol, has a low partition coefficient to *n*-butanol (3.2) and high viscosity (28.3 cP). Additionally, to prevent emulsion formation, the extractant and fermentation phases cannot be mixed vigorously, which makes achieving interphase mass transfer challenging. The recovery rate is therefore relatively low, resulting in low productivity (Table S2, ESI†). To overcome the low productivity of LL processing, membrane-based extraction, also referred to as perstraction (PS, Fig. 1f), has been explored. A membrane is placed between two immiscible liquids to extract the produced alcohol while protecting micro-organisms from high partition coefficient extractants which are toxic to micro-organisms. This system has advantages such as (a) high driving force (high partition coefficient), (b) effective processing conditions (minimized concentration polarization due to high circulation) and (c) favourable scale up (modularity).[15,22–24] In spite of all these advantages, the PS technology has remained immature to date, due to the high mass transfer resistance through state-of-the-art membranes (Table S2, ESI†).[22,25] This study presents a solution to this longstanding problem of affinity-driven membrane separation by focusing our research on the three key areas of extractant, membrane, and engineering. We have created new membranes with an order of magnitude improvement in higher alcohol fluxes, leading to an innovative perstraction platform combining these membranes with extractants to improve productivity over previous systems by more than a factor of 10 (Table S2, ESI†), while simultaneously lowering energy intensity to 3.9 MJ kg^{-1}, Table S3 and S4 (ESI†). Moreover, this research platform broadens the general applicability of PS for organic chemicals produced by fermentation (where it can ''shield'' microorganisms from extractant toxicity), through to challenging separations such as multi-ring aromatic hydrocarbons, crude reaction products and others (Appendix S1, ESI†).

2. Results and discussion

A high partition coefficient (P) of extractant is desirable in perstraction to increase effective driving force ($\Delta C^{i}_{eff} = PC^{i}_{fe} - C^{i}_{ex}$) and thereby improve productivity. Though most extractants having high partition coefficients are toxic to the fermentation organisms or exist in the solid-state, their use in the perstraction does not affect the organism which can be protected from direct exposure by the membrane. We considered six potential extractants which are immiscible with water (Table S5, ESI†), determining partition coefficients for linear and branched propanol, butanol, and pentanol following OECD guideline 107. All extractants showed the same trend of increasing partition coefficient for higher alcohols (Fig. S2a, ESI†). The most common extractants in liquid–liquid extraction for ethanol production, oleyl alcohol and tributyrin, have partition coefficients for *n*-butanol ($P^{n\text{-BuOH}}$) of 3.6 and 2.2 respectively. In contrast, 2-ethyl-1-hexanol and 1-dodecanol, which are relatively toxic to the micro-organisms, showed higher partition coefficients of 9.3 and 6.0, respectively.[26,27] Since 2-ethyl-1-hexanol (2EH) has attractive properties for perstraction including: (a) low viscosity (less concentration polarization); (b) low heat capacity (less energy consumption during distillation); (c) inexpensive and readily available (annual production 3.3×10^{6} tons); (d) high partition coefficient; and (e) has low volatility and does not form an azeotrope with alcohols, 2EH is chosen for further study with oleyl alcohol (OA) as a control material. Both 2EH and OA showed the same partition coefficient trends with isomers Fig. S2b (ESI†). Although the partition coefficients for branched alcohols ($P^{i\text{-BuOH}}_{2EH} = 7.5$ and $P^{i\text{-PnOH}}_{2EH} = 23.6$, respectively) are lower than those of linear alcohols ($P^{n\text{-BuOH}}_{2EH} = 9.3$ and $P^{n\text{-PnOH}}_{2EH} = 35.9$), they are still higher than those with OA ($P^{n\text{-PnOH}}_{OA} = 3.6$ and $P^{i\text{-PnOH}}_{OA} = 10.9$). Crucially however, because 2EH inhibits metabolism of the micro-organisms, to exploit the excellent partitioning properties, a membrane is required to protect the micro-organisms during alcohol production with *in situ* recovery.

To maintain a stable interface between water (fermentation broth) and extractant while promoting alcohol extraction, the affinity of the membrane material must be tailored to the three liquids in the system (water, alcohol, and extractant). Searching for a suitable material, we tested four different membranes having different separating layers: a porous membrane, crosslinked polyamide (×PA) membrane, a crosslinked polydimethylsiloxane (×PDMS) composite membrane, and a crosslinked sulfonated poly(arylene ether sulfone) (×SPAES) thin-film composite membrane (Fig. 2a–d). The porous membrane represents a control sample without any separating layer (defective membrane areas are included). ×PA ($\delta = 29$ $MPa^{1/2}$) and ×PDMS ($\delta = 15$ $MPa^{1/2}$) membranes are the most common representatives of hydrophilic and hydrophobic membranes respectively which have been reported in the literature.[33,34] In contrast, the ×SPAES membrane has an intermediate affinity ($\delta = 25$ $MPa^{1/2}$). The thin-film composite membranes were prepared with thinner than 1 μm separating layers on the porous support *via* appropriate fabrication methods (interfacial polymerization, gravure coating, and spray coating)

 This journal is © The Royal Society of Chemistry 2020

Open Access Article. Published on 24 October 2020. Downloaded on 3/12/2021 3:23:00 PM.
This article is licensed under a Creative Commons Attribution-NonCommercial 3.0 Unported Licence.

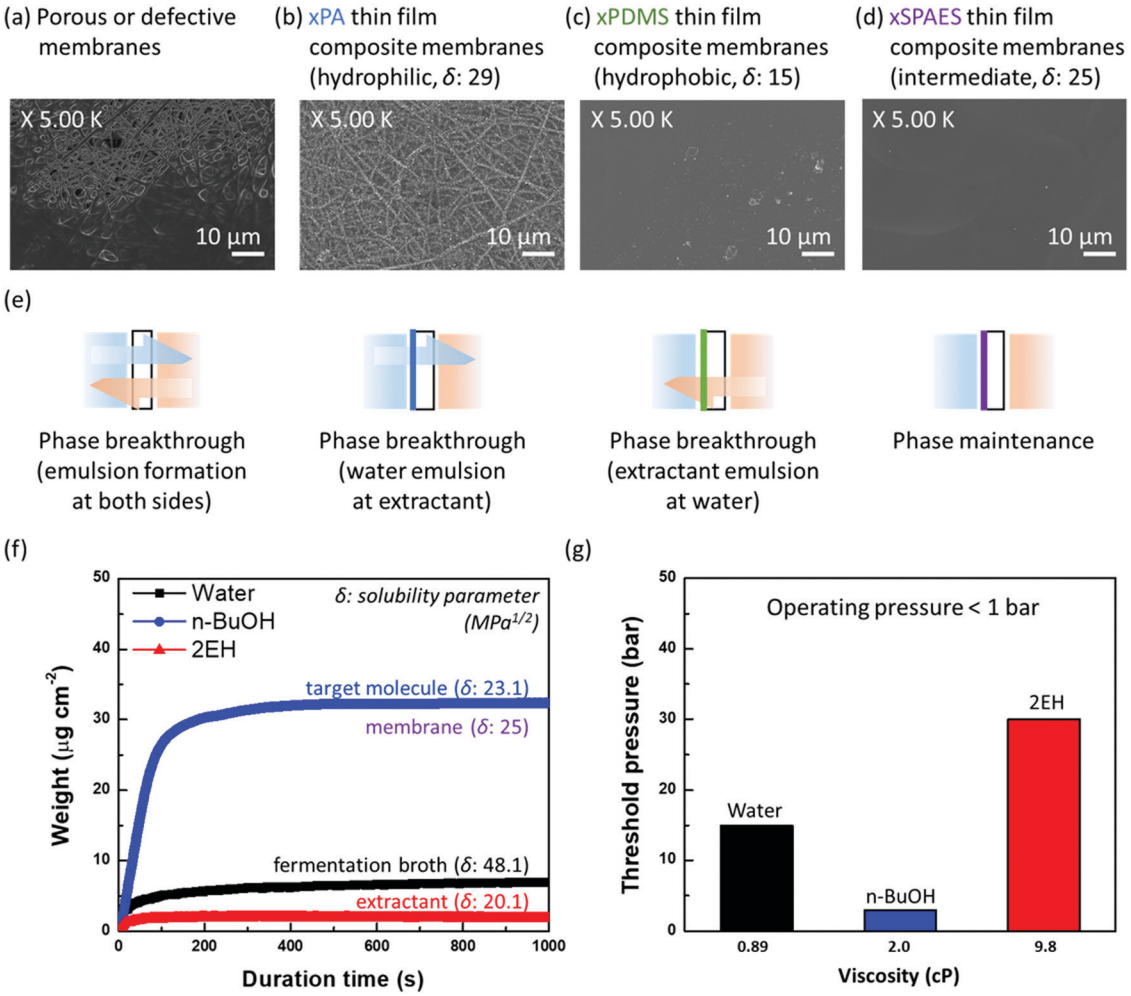


Fig. 2 Surface SEM images of the membranes fabricated in this study: (a) a porous membrane (defective sections included), (b) crosslinked polyamide (×PA), (c) crosslinked polydimethylsiloxane (×PDMS), and (d) crosslinked sulfonated poly(arylene ether sulfone) (×SPAES) thin film composite membranes. The cross-sectional images can be seen in Fig. S3 (ESI†). (e) Schematic diagrams of differences in the interfacial behaviour between water and extractant through the fabricated membranes. Tests were conducted using a cross-flow system (Fig. S4, ESI†) and the schematics are based on the digital photographs obtained (Fig. S5, ESI†). (f) Adsorption profiles of the ×SPAES membrane with water, *n*-butanol, and 2-ethyl-1-hexanol, obtained using a quartz crystal microbalance (QCM). Measurements were conducted by immersing a probe into each solvent separately at 37 °C. (g) Threshold (phase breakthrough) pressures of the ×SPAES membrane were measured with a dead-end filtration apparatus separately for each solvent with nitrogen gas (Section S3, ESI†).[28–32]

depending on the materials (×PA, ×PDMS, and ×SPAES), respectively (Fig. S3 and Section S3, ESI†).[28–32] Performance of the fabricated membranes was investigated using a cross-flow system with pure water and 2EH flowing counter-currently at 1.0 L min^{-1} (0.16 m s^{-1}) (Fig. S4, ESI†). As shown in Fig. 2e and Fig. S5a (ESI†), the porous or defective membranes readily formed emulsions in both solutions, since they present no barrier to prevent the transfer of water and extractant molecules. In Fig. S5b and c (ESI†), ×PA and ×PDMS membranes did not form emulsions immediately, however each membrane allowed a favourable solvent system to go pass through and form an emulsion after operation for longer than 12 h. The ×PA membrane generated a water emulsion in the extractant solution, in contrast to the ×PDMS membrane which formed an extractant emulsion in the water solution (Fig. 2e). Although the dense separating layer can delay emulsion formation during initial operation, a system in which one of the major fluids has close affinity to the membrane material will eventually allow that liquid to permeate the membrane, and form an emulsion in the other phase. On the other hand, ×SPAES, having an intermediate affinity between ×PA and ×PDMS was able to stabilise the interface between water and 2EH without any emulsion formation on either side over more than 24 h operation (Fig. S5d, ESI†). It is essential to avoid emulsion formation on both sides of membranes, as extractant migration to the aqueous side will result in inhibition of the fermentation, while water migration to the extractant side will complicate the subsequent separation process.

To further explore underlying interfacial phenomena enabling successful stabilisation of the interface by ×SPAES, liquid sorption isotherms and breakthrough pressures of ×SPAES with three solvents (water, 2EH and *n*-butanol) were measured at 37 °C using quartz crystal microbalance and dead-end filtration test,

Open Access Article. Published on 24 October 2020. Downloaded on 3/12/2021 3:23:00 PM.
This article is licensed under a Creative Commons Attribution-NonCommercial 3.0 Unported Licence.

respectively. In Fig. 2f, ×SPAES showed slow adsorption and low adsorption capacity against water and 2EH. In contrast, for a representative biofuel (*n*-butanol, *n*-BuOH), ×SPAES exhibited ten times faster adsorption rate (dw/dt) for *n*-BuOH (0.35 μg cm^{-2} s^{-1}) than water (0.034 μg cm^{-2} s^{-1}) and 2EH (0.012 μg cm^{-2} s^{-1}) at early stages of the test before saturation level. These data reveal a strong correlation with the affinity differences between ×SPAES and the three liquids. In Fig. 2e, ×SPAES showed higher threshold pressures to all liquids than the perstraction system operating pressure, which is less than 1 bar. Although *n*-BuOH has a viscosity (2.0 cP) more than twice that of water (0.89 cP), ×SPAES showed a much lower threshold pressure for *n*-BuOH (3 bar) than water (15 bar). Crucially, since the perstraction system operates based on concentration difference, the high threshold pressures of ×SPAES toward the two bulk liquids (water and 2EH) promoted a stable interface with no emulsion formation, enabling smooth, continuous extraction of *n*-BuOH.

To verify the potential of ×SPAES to improve biofuel production, membrane performance was investigated first with synthetic binary mixtures and then a model fermentation broth. For the former, dynamic test conditions with 200 ml of 1 wt% *n*-BuOH aqueous solution and two pure extractants (2EH and OA) were employed. Fig. 3a shows the recovery ratio (%) (ratio between the final mass of extracted alcohol to the initial mass of alcohol in the feed) as a function of time for both extractants. 2EH exhibited five times faster recovery rate for the first 20 hours of operation than OA due to the higher partition coefficient for *n*-BuOH ($P_{2EH}^{n\text{-BuOH}}$ = 9.3) than OA ($P_{OA}^{n\text{-BuOH}}$ = 3.6). These experiments also illustrated that alcohols from the feed solution can be extracted up to the equilibrium partition concentration between aqueous and extraction phases (dashed lines in Fig. 3a), regardless of the presence of the membrane, and without any phase breakthrough occurring. Therefore, to provide the highest alcohol productivity, 2EH was used as the extractant for further experiments. Butanol flux of the ×SPAES membrane was investigated

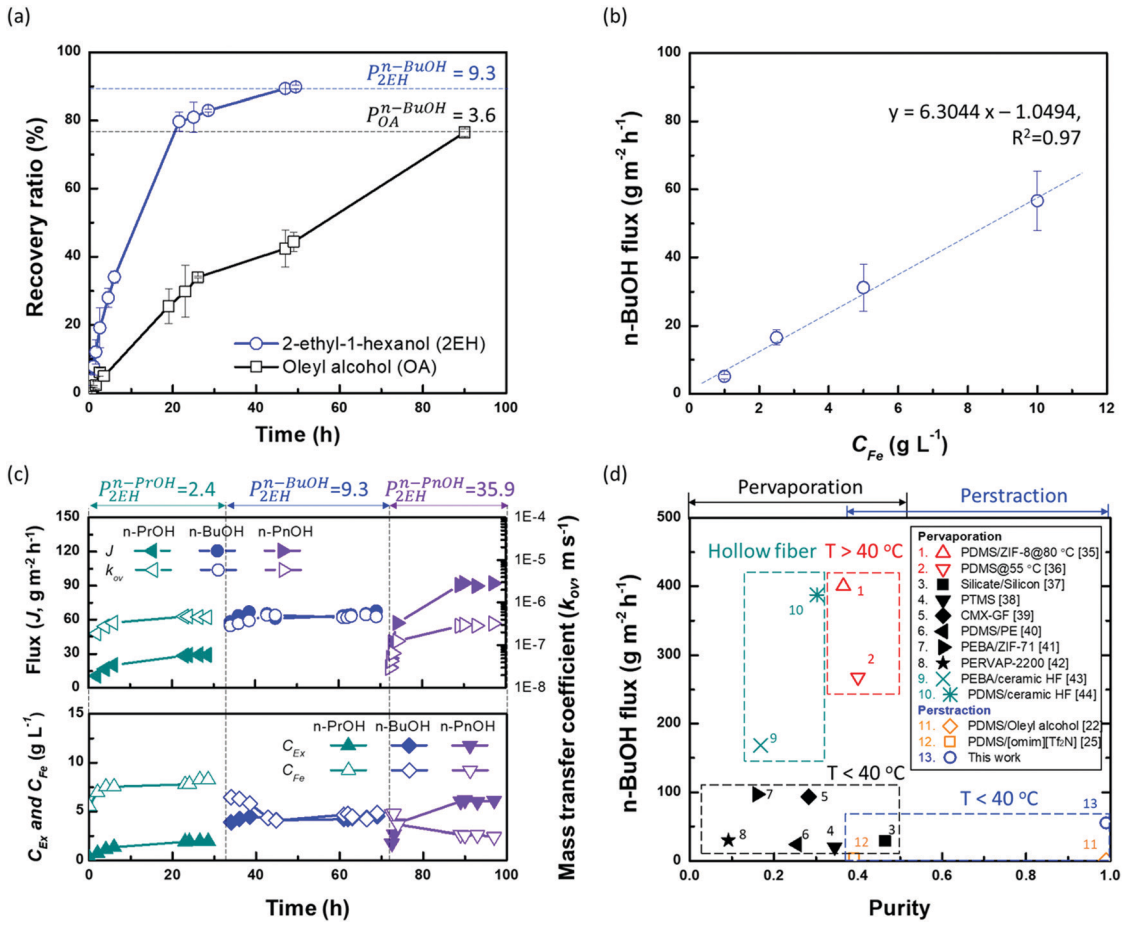


Fig. 3 (a) Recovery ratio (RR%) of the ×SPAES membrane with equal 200 ml volumes of 1 wt% *n*-butanol (*n*-BuOH) aqueous solution as feed and either pure 2-ethyl-1-hexanol (2EH, $P_{2EH}^{n\text{-BuOH}}$ = 9.3) or pure oleyl alcohol (OA, $P_{OA}^{n\text{-BuOH}}$ = 3.6) as extractant. The dashed lines represent the theoretical maximum concentration of the extractable *n*-BuOH in each extractant ($RR^{Theo.Max.} = P/(1+P)$). (b) Perstraction flux through ×SPAES membrane in dynamic tests with 1 L each of (i) pure 2EH and (ii) aqueous butanol solution with 0.1, 0.25, 0.5, and 1.0 wt% *n*-BuOHaq. The butanol concentration profiles over time is provided in Fig. S6 (ESI†). (c) Steady-state performance of the ×SPAES membrane with three target molecules *n*-propanol (*n*-PrOH, $P_{2EH}^{n\text{-PrOH}}$ = 2.4); *n*-butanol (*n*-BuOH, $P_{2EH}^{n\text{-BuOH}}$ = 9.3; and *n*-pentanol (*n*-PnOH, $P_{2EH}^{n\text{-PnOH}}$ = 35.9) with 1.0 wt% concentration. Each test was conducted after washing the system with pure 2EH (extractant side) and water (feed side). (d) Performance comparison between the ×SPAES membrane and the membrane-based processes (pervaporation and perstraction) reported in the literature (Table S2, ESI†).[22,25,35–44]

 This journal is © The Royal Society of Chemistry 2020

Open Access Article. Published on 24 October 2020. Downloaded on 3/12/2021 3:23:00 PM.
This article is licensed under a Creative Commons Attribution-NonCommercial 3.0 Unported Licence.

with feed solutions with *n*-BuOH concentrations varying from 0.1, 0.25, 0.5 to 1 wt% in aqueous solution (Fig. 3b and Fig. S6, ESI†). The butanol flux ($\dot{J}$, g m^{-2} h^{-1}) was calculated from eqn (1) (Section S4, ESI†).[45]

$$\dot{J} = \dot{N}/A = \frac{V_{Ex}}{A}\frac{d\dot{C}_{Ex}}{dt} = \frac{V_{Ex}}{A}\frac{C_{Ex,t} - C_{Ex,0}}{t} = \dot{k}_{ov}\left(P \cdot C_{Fe,t} - C_{Ex,t}\right) \quad (1)$$

where $\dot{N}$ is mass flux and A is an active membrane area, V_{Ex} is a volume of extractant, $C_{Ex,t}$ and $C_{Ex,0}$ are alcohol concentrations of extractant at time 't' and '0', respectively; P is the partition coefficient, $\dot{k}_{ov}$ is an overall mass transfer coefficient.

The butanol flux was strongly correlated to the aqueous butanol concentration (dashed line in Fig. 3b), as expected for a process driven by concentration difference. The ×SPAES membrane exhibited one-order of magnitude higher butanol flux (55 g m^{-2} h^{-1}) than the previously reported PDMS membranes which were operated with the same feed concentration using either [$P_{6,6,6,14}$][DCA] (5.5 g m^{-2} h^{-1}) and OA (1 g m^{-2} h^{-1}) as extractants.[22,25] This is attributed primarily to the new ×SPAES membrane having a much thinner effective diffusion length than the previously employed PDMS membranes and higher affinity towards *n*-BuOH (Fig. 2f); and also to the lower viscosity (9.8 cP) and higher partition coefficient of 2EH. To explore the general applicability of the platform to higher alcohols, the intrinsic membrane performance of ×SPAES was further investigated with three target alcohols having different partition coefficients: *n*-PrOH, *n*-BuOH, and *n*-PnOH (Fig. 3c). These steady state tests were performed with 100 ml each of 1 wt% the target alcohol aqueous solution as feed and pure 2EH as extractant, with both liquids circulating at 1.0 L min^{-1} (0.16 m s^{-1}) in counter-current flow through the membrane module. Constant flows of fresh aqueous feed and pure 2EH at 0.5 ml min^{-1} each were supplied to the feed and extractant reservoirs (Fig. S7, ESI†), with overflow maintaining a constant volume in the system. When constant concentration was reached at each side ($dC/dt = 0$), the membrane flux and overall mass transfer coefficient at steady-state were calculated using eqn (2) (Section S4, ESI†).[46]

$$\dot{J} = \dot{N}/A = \frac{C_{Ex}}{A}\dot{F}_{Ex} = \dot{k}_{ov}\frac{F_{Fe}}{F_{Ex}}(P \cdot C_{Fe} - C_{Ex}) \quad (2)$$

where F_{Ex} and F_{Fe} are dosing rate of extractant and feed solutions to each reservoir.

The concentrations in feed and extractant become constant at steady state after around 25 h operation for each alcohol. Since higher alcohols have higher partition coefficients, alcohol flux of ×SPAES increased from 30 g m^{-2} h^{-1} with *n*-PrOH, to 65 g m^{-2} h^{-1} with *n*-BuOH, and to 90 g m^{-2} h^{-1} with *n*-PnOH (Fig. 3c). In contrast, the overall mass transfer coefficient was 5.0 × 10^{-7} m s^{-1} for both *n*-PrOH and *n*-BuOH but decreased to 3.0 × 10^{-7} m s^{-1} with *n*-PnOH. To evaluate which is the main resistance determining mass transfer coefficient, a resistance in-series model (Fig. S8, ESI†) is employed as in eqn (3):

$$\frac{J}{\dot{k}_{ov}} = \frac{P \cdot J}{\dot{k}_{Fe}} + \frac{J}{\dot{k}_{m}} + \frac{J}{\dot{k}_{Ex}} = P\left(C_{Fe,b} - C_{Fe,m}\right) + \left(PC_{Fe,m} - C_{Ex,m}\right) + \left(C_{Ex,m} - C_{Ex,b}\right) \quad (3)$$

where $\dot{k}_{Fe}$ and $\dot{k}_{Ex}$ are mass transfer coefficients of liquid films (feed and extractant), $\dot{k}_{m}$ is the effective mass transfer coefficient of the membrane, $C_{Ex,b}$ and $C_{Ex,m}$ are alcohol concentration in the bulk extractant phase and membrane surface on extractant side, $C_{Fe,b}$ and $C_{Fe,m}$ are alcohol concentration in the bulk feed phase and membrane surface on feed side, respectively.

Liquid film mass transfer coefficients for *n*-BuOH were estimated using eqn (S16) (ESI†).[47] Contributions of each resistance were calculated from eqn (S17)–(S19) (ESI†). The extractant-side mass transfer coefficient of *n*-BuOH (k_{Ex} = 2.6 × 10^{-6} m s^{-1}) is lower than that in water (k_{Fe} = 6.8 × 10^{-6} m s^{-1}). Since the liquid film mass transfer coefficients are both an order of magnitude higher than the overall mass transfer coefficient (k_{ov} = 5.0 × 10^{-7} m s^{-1}), the major contribution to the overall mass transfer resistance is in the membrane (γ_m) which accounts for >70% of total resistance regardless of target alcohols (Table S6, ESI†). The contribution of extractant-side (γ_{Ex}) which was 12–20% of the total, is much higher than that of feed-side (γ_{Fe}). For *n*-PnOH, the contribution of membrane resistance was as high as 81%, compared *n*-PrOH (76%) and *n*-BuOH (74%). This is attributed to the lower affinity of pentanol for the membrane (solubility parameter of *n*-butanol δ =23.3; *n*-propanol δ = 24.6; *n*-pentanol δ = 21.7 *vs.* membrane δ = 24.9 MPa$^{1/2}$), and to greater concentration polarization due to the higher flux through the membrane, especially because the porous support of the composite membrane is facing the organic phase, and the porous support will contribute significantly toward the mass transfer resistance.[48,49] Therefore, while this perstraction system exhibits significantly higher fluxes than current state-of-the-art, minimizing the concentration polarization has potential to further boost productivity. One possible approach is to increase the operating temperature at the extractant site, thus reducing viscosity and enhancing mass transfer. This option will be discussed further below in the context of synthetic fermentation broth simulating *in situ* recovery of butanol. In Fig. 3d, the performance of ×SPAES membrane for *n*-BuOH is compared to the state-of-the-art membranes reported in the literature with a binary mixture.[22,25,35–44] The pervaporation membranes typically show high *n*-BuOH flux with average selectivity less than 100 (Table S2, ESI†). Considering the conventional fed-batch fermentation cannot produce higher than 1.2 wt% concentration of *n*-BuOH, the *n*-BuOH aqueous solution at a condenser achievable by the state-of-the-art membranes is at maximum ~50 wt%. The pervaporation system also requires significant energy to heat up the solution, and subsequently to carry out the heterogeneous azeotropic distillation. Although increasing the operating temperature of the pervaporation system enhances productivity, selectivity of the system could not be improved (Table S2, ESI†). In contrast, previously reported

Open Access Article. Published on 24 October 2020. Downloaded on 3/12/2021 3:23:00 PM.
This article is licensed under a Creative Commons Attribution-NonCommercial 3.0 Unported Licence.

perstraction systems have shown low productivity, but with outstanding selectivity. Herein, by introducing the well-tailored combination of ×SPAES with 2EH, we have improved *n*-BuOH productivity of the perstraction system ten-fold in comparison with the previous systems, crucially without compromising selectivity. This high selectivity reduces the energy consumption to regenerate the extracted alcohols to fuel-grade because simple distillation can be employed, and because 2EH has lower heat capacity (2.45 J g^{-1} K^{-1}) and lower vapour pressure (0.07 bar at 391 K; the boiling point of *n*-BuOH) than water (4.18 J g^{-1} K^{-1} and 0.7 bar at 364.3 K; heterogeneous azeotrope temperature). Furthermore, since the perstraction system can operate with extractant-to-feed solution volumes less than 0.5, because the partitioning into 2EH is so favourable, and the SPAES membrane avoids the toxic effect of the extractant (Table S4, ESI†), the energy requirements are further reduced compared to the conventional direct-contact liquid–liquid extraction and dehydration processes.[15,16]

The effects of extractant : feed volume ratio (V_{Ex}/V_{Fe}) and recovery factor (%) on perstraction for continuous butanol production at steady state were assessed based on eqn (4) and (5) (Section S5, ESI†):

$$\frac{d\dot{C}_{Ex}}{dt} = \frac{\dot{k}_{ov} \cdot A}{V_{Ex}}\left[P \cdot \left\{C_{Fe,0} - \frac{V_{Ex}}{V_{Fe}}\left(C_{Ex,t} - C_{Ex,0}\right)\right\} - C_{Ex,t}\right] \quad (4)$$

$$C_{Ex,t}^{RF} = RF \times \frac{C_{Fe,0} \cdot P}{1 + P \cdot \frac{V_{Ex}}{V_{Fe}}} \mathrm{RF(Recovery\ Factor)} = 0.1,\ 0.3,\ 0.5,\ \text{and}\ 0.99 \quad (5)$$

Continuous butanol production with perstraction was designed at a steady-state condition with a constant mass flow of butanol in all three components: fermentation broth (production rate); perstraction (recovery rate); and distillation column (production rate) (Fig. S10, ESI†). The volume ratio (V_{Ex}/V_{Fe}) and recovery factor (RF) were controlled from 0 to 1 under assumptions including (i) constant feed volume (V_{Fe} = 10 L) and concentration ($C_{Fe,0}$ = 1 wt% *n*-$BuOH_{aq}$) as a fed-batch fermentation, (ii) overall mass transfer coefficient (k_{ov}, 5.0 × 10^{-7} m s^{-1}) and membrane area (1 m^2), (iii) initial and saturated extractant concentrations ($C_{Ex,0}$ = 0 and $C_{Ex,t}^{RF}$ at each V_{Ex}/V_{Fe} and RF), and (iv) extractant is recycled after distillation. In Fig. 4a and Fig. S10a (ESI†), the recovery rate (dC_{Ex}/dt) showed a dramatic decline as volume ratio (V_{Ex}/V_{Fe}) increases. As can be seen in eqn (4), since the driving force is reduced with V_{Ex} increment, recovery rate decreased as the volume ratio increased. The 0.99 recovery rate shows the most significant change. It represents extraction of the alcohol from the fermentation broth almost up to saturation level (99%) of extractant, has low concentration difference and consequently is not favourable for the continuous process due to the low production rate. Though the low V_{Ex}/V_{Fe} and RF appears desirable in terms of recovery rate, lower RF would require more energy to heat extractant to produce butanol in the distillation column. Therefore, energy consumption and process time per unit butanol production at each condition were calculated to determine optimum conditions (Section S5, ESI†).

The mass flow of butanol (dw_{Ex}/dt) from fermentation broth, in perstraction, and in the distillation column is the same at each RF regardless of V_{Ex}/V_{Fe} (Fig. S10b, ESI†). The process time per unit kg of butanol production can be estimated at each RF (Fig. S10c, ESI†). To simulate the energy consumption, the feed streams to distillation column at each V_{Ex}/V_{Fe} and RF were controlled to maintain a steady-state. All simulation conditions and results are tabulated in Table S7 (ESI†). Energy consumptions decrease when RF increases because the feed stream contains high butanol concentration (Fig. 4b). The change of energy consumptions at low V_{Ex}/V_{Fe} according to RF is less sensitive than that at high V_{Ex}/V_{Fe} due to less heating energy. However, since the mass flow of butanol at high RF is significantly reduced, it requires longer process times (Fig. S10c, ESI†). To determine an optimum condition for the minimum energy consumption and process time, the energy consumptions at each V_{Ex}/V_{Fe} were plotted with the process time (Fig. 4c). The process time (6.6, 8.5, 11.9, and 597.4 h kg^{-1}) corresponds to RF (0.1, 0.3, 0.5, and 0.99) (Fig. S10b, ESI†). The minimum condition can be found with the lowest area of energy consumption x process time (Table S7, ESI†). The lowest energy consumption is 3.69 MJ kg^{-1} at 0.001 of V_{Ex}/V_{Fe} at RF = 0.99. However, it requires very much longer process time (597.4 h kg^{-1}) than the shortest process time (6.6 h kg^{-1}). In contrast, the shortest process time at 0.001 of V_{Ex}/V_{Fe} and 0.1 of RF requires four times higher energy consumption (22.77 MJ kg^{-1}) than the lowest energy consumption. Though a process with the lowest energy consumption requires longer process times, it may be suitable for batch processes. Although the lower V_{Ex}/V_{Fe} is favourable in terms of the energy consumption, from the practical point of view, less than 0.01 of V_{Ex}/V_{Fe} (0.1 L of V_{Ex}) does not provide sufficient extractant to fill the perstraction system and distillation column. Therefore, a practical condition for continuous butanol production, balancing energy consumption with rate, is in the region of 6.46 MJ kg^{-1} and 11.9 h kg^{-1} at 0.01 of V_{Ex}/V_{Fe} and 0.5 of RF. We note that if the continuous perstraction system is scaled up (V_{Fe}), removing the extractant volume constraint, the energy consumption could be reduced with smaller volume ratio (V_{Ex}/V_{Fe}) than 0.01.

In Fig. 4d, the energy consumption of perstraction through ×SPAES membranes with the optimum volume ratio (0.01, V_{Ex}/V_{Fe}) and recovery factor (50%, RF) was compared to other recovery systems including flash, vacuum distillation, gas stripping, pervaporation and liquid–liquid extraction.[15–17,19,50] The energy consumption for direct distillation showed the highest value due to the requirement for heterogeneous azeotropic distillation directly from a low concentration fermentation broth (1 wt%) *n*-$BuOH_{aq}$. Although energy consumption of this option decreases as feed butanol concentration increases, it still requires up to 10 MJ kg^{-1} even at 80 wt% feed concentration.[17,50] Dehydration processes such as gas stripping and pervaporation showed lower energy consumptions than direct distillation. However, both require the use of highly energy-intensive stages for dehydration of butanol solution

 This journal is © The Royal Society of Chemistry 2020

Open Access Article. Published on 24 October 2020. Downloaded on 3/12/2021 3:23:00 PM.
This article is licensed under a Creative Commons Attribution-NonCommercial 3.0 Unported Licence.

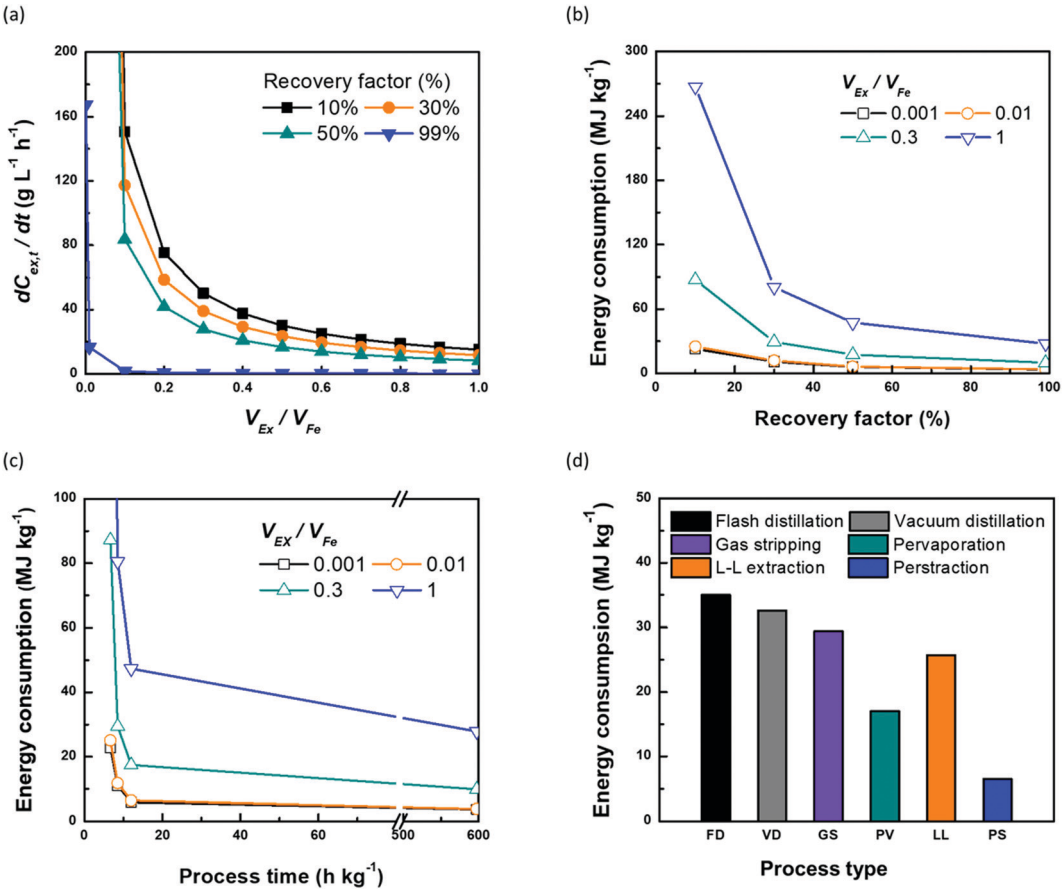


Fig. 4 The effect of volume ratio of extractant : feed (V_{Ex}/V_{Fe}) and recovery factor (RF) on the continuous perstraction system in terms of (a) recovery rate (dC_{Ex}/dt, g L^{-1} h^{-1}) and energy consumption (MJ kg^{-1}) according to (b) recovery factor (%) and (c) process time (h kg^{-1}). The simulations were performed based on 1 wt% of 10 L *n*-BuOHaq feed solution and 1 m^2 membrane area with 5.0 × 10^{-7} m s^{-1} overall mass transfer coefficient using eqn (4) and (5) (the details are described in Section S5, and Fig. S6 (ESI†). (d) Comparison between the recovery systems of energy consumption per kg production of *n*-BuOH. For (d), the energy consumption of perstraction was chosen at the lowest feasible extractant : feed volume ratio (0.01, V_{Ex}/V_{Fe}) and recovery factor (50%) which corresponds to the lowest energy consumption and time (Tables S3 and S7, ESI†).

through phase changes, and further heterogeneous azeotropic distillation of the condensed *n*-BuOH-aqueous solution. Extraction followed by distillation from the extractant can produce *n*-BuOH with lower energy consumption than direct distillation and dehydration processes because no phase change is required for the first stage, and the distillation required to recover the alcohols from extractant at the second stage is considerably simpler than the distillation required to recover alcohols from aqueous solution. However, direct contact liquid–liquid extraction systems must select extractants from a limited range, constrained by extractant toxicity to the fermentation organisms. This in turn limits the obtainable partition coefficient and increases required extractant : feed volume ratio[16,51] Finally, combining the innovative ×SPAES membrane with microbially-toxic-under-direct-contact but highly selective 2EH extractant offers a route to both reduce the energy footprint of biofuel production, and enhance productivity, and is by some way the most energy efficient option.

To investigate the potential of the developed system under realistic operating conditions, Clostridium acetobutyricum (ATCC 824) was inoculated to a bioreactor (Appendix S5, ESI†). The anaerobic fermentation was conducted until the broth reached an optical density of 8.0 at 600 nm ($O.D._{600}$) which represents a fully grown population of the micro-organisms (Section S6, ESI†).[51] For consistency with the energy consumption calculations, the *n*-BuOH concentration was artificially adjusted to 1 wt% to simulate manufacturing conditions. Perstraction tests were conducted with the adjusted fermentation broth and pure 2EH (Fig. S11a, ESI†), and showed successful performance with no emulsification, albeit at somewhat reduced mass transfer rates, due to the biofouling of membrane.[15] Because typical biofuel production often includes integrated cell separation/recovery, or cell-immobilization, a further test with the fermentation broth filtered through a 0.45 μm filter was conducted to simulate this operating mode (Fig. S11b, ESI†). The filtered solution can be considered representative of an immobilized cell fermentation broth, which continues to show effects of accumulating solutes such as carboxylic acids and glucose on the membrane surface.[52] The test with a filtered broth ($O.D._{600}$ = 3.5) showed a recovery flux significantly closer to that measured for a binary mixture (Fig. S11c, ESI†). The *n*-BuOH extracted into 2EH from the filtered broth was

Open Access Article. Published on 24 October 2020. Downloaded on 3/12/2021 3:23:00 PM.
This article is licensed under a Creative Commons Attribution-NonCommercial 3.0 Unported Licence.

regenerated with a Vigreux column (Fig. S12, ESI†). The distillate showed high purity of *n*-BuOH, with no traces of water or 2EH. Further tests were performed to evaluate the extent of "shielding" provided by the membrane against extractant toxicity towards the micro-organisms. A Hungate tube test using a one-day incubation during the cell propagation step revealed that the ×SPAES membrane fully protected cells from 2EH (Fig. S13, ESI†).

The above results suggest that this perstraction system could be employed as a continuous process for biofuel manufacturing consisting of production of alcohols in the fermentation broth with *in situ* recovery at elevated extractant temperatures; followed by regeneration of the extracted alcohols through distillation – all simultaneously operated in continuous mode (Fig. S9, ESI†). This approach would bring three additional advantages: (a) the recovery rate would be higher when extractant temperature increases from 37 °C to 70 °C since the viscosity of 2EH decreases from 9.8 cP to 2.69 cP while partition coefficient remains nearly constant ($P_{2EH}^{n\text{-BuOH}}$ = 8.2 at 70 °C); (b) the recovery rate would be maximized by reducing extractant alcohol concentration by distillation, and; (c) the system yield would be improved by maximizing alcohol production over the same fermentable resource. Thus the developed perstraction system with ×SPAES and 2EH offers a promising perspective for biofuel production with high productivity and low energy consumption.

3. Conclusion

In this study, a perstraction system for the production of fuel grade bio-alcohols was developed, comprising (a) liquid systems (extractants and target molecules), (b) membrane materials, and (c) engineering design. Criteria for extractant selection were considered in terms of their impacts on energy consumption and toxicity to microbial metabolism in the fermentation. 2-Ethyl-1-hexanol was selected as an extractant since it exhibits three times higher partition coefficients for higher alcohols and their isomers than state-of-the-art direct liquid contact extractants. The toxicity of 2EH towards micro-organisms was overcome by creating a novel membrane with tailored affinity toward the three liquid systems (water, extractant, and alcohol). These ×SPAES membranes successfully protect the micro-organisms from the extractant and simultaneously extract the produced alcohols without any emulsification. This was shown to be an excellent compromise within the ternary liquid system; *n*-BuOH flux through the ×SPAES membrane is one-order of magnitude higher than for state-of-the-art perstraction systems, without compromising an excellent *n*-BuOH/water selectivity. Engineering perspectives of the perstraction system with ×SPAES and 2EH were investigated and it is found that the energy consumption can be reduced to less than one-quarter that of conventional recovery systems, by controlling parameters including the extractant : feed volume ratio. Thus the developed perstraction system with ×SPAES and 2EH offers a promising perspective for biofuel production with high productivity and low energy consumption.

Conflicts of interest

There are no conflicts to declare.

Acknowledgements

This research was supported by BP through the BP International Centre for Advanced Materials (BP-ICAM) and Basic Science Research Program through the National Research Foundation of Korea (NRF) funded by the Ministry of Education (2018R1A6A3A03012680).

References

1 M. M. Thackeray, C. Wolverton and E. D. Isaacs, *Energy Environ. Sci.*, 2012, **5**, 7854.
2 J. C. Liao, L. Mi, S. Pontrelli and S. Luo, *Nat. Rev. Microbiol.*, 2016, **14**, 288–304.
3 C. Beer, M. Reichstein, E. Tomelleri, P. Ciais, M. Jung, N. Carvalhais, C. Rodenbeck, M. A. Arain, D. Baldocchi, G. B. Bonan, A. Bondeau, A. Cescatti, G. Lasslop, A. Lindroth, M. Lomas, S. Luyssaert, H. Margolis, K. W. Oleson, O. Roupsard, E. Veenendaal, N. Viovy, C. Williams, F. I. Woodward and D. Papale, *Science*, 2010, **329**, 834–838.
4 P. Fairley, *Nature*, 2011, **474**, S2–5.
5 H. Olcay, R. Malina, A. A. Upadhye, J. I. Hileman, G. W. Huber and S. R. H. Barrett, *Energy Environ. Sci.*, 2018, **11**, 2085–2101.
6 H. E. Murdock, D. Gibb, T. André, F. Appavou, A. Brown, B. Epp, B. Kondev, A. McCrone, E. Musolino and L. Ranalder, Renewables 2019 Global Status Report, Report ISBN 978-3-9818911-7-1, 2019.
7 T. B. Bonenkamp, L. M. Middelburg, M. O. Hosli and R. F. Wolffenbuttel, *Renewable Sustainable Energy Rev.*, 2020, **120**, 109667.
8 C. P. Hubbard, J. E. Anderson and T. J. Wallington, *Environ. Sci. Technol.*, 2014, **48**, 861–867.
9 S. Atsumi, T. Hanai and J. C. Liao, *Nature*, 2008, **451**, 86–89.
10 M. Vinod Babu, K. Madhu Murthy and G. Amba Prasad Rao, *Renew. Sust. Energ. Rev.*, 2017, **78**, 1068–1088.
11 N. Savage, *Nature*, 2011, **474**, S9–11.
12 L. da Costa Sousa, M. Jin, S. P. S. Chundawat, V. Bokade, X. Tang, A. Azarpira, F. Lu, U. Avci, J. Humpula, N. Uppugundla, C. Gunawan, S. Pattathil, A. M. Cheh, N. Kothari, R. Kumar, J. Ralph, M. G. Hahn, C. E. Wyman, S. Singh, B. A. Simmons, B. E. Dale and V. Balan, *Energy Environ. Sci.*, 2016, **9**, 1215–1223.
13 E. I. Lan, S. Y. Ro and J. C. Liao, *Energy Environ. Sci.*, 2013, **6**, 2672.
14 A. Nalaparaju, X. S. Zhao and J. W. Jiang, *Energy Environ. Sci.*, 2011, **4**, 2107.
15 P. Jimenez-Bonilla and Y. Wang, *Crit. Rev. Biotechnol.*, 2018, **38**, 469–482.
16 V. Outram, C. A. Lalander, J. G. M. Lee, E. T. Davis and A. P. Harvey, *Bioresour. Technol.*, 2016, **220**, 590–600.

 This journal is © The Royal Society of Chemistry 2020

Open Access Article. Published on 24 October 2020. Downloaded on 3/12/2021 3:23:00 PM.
This article is licensed under a Creative Commons Attribution-NonCommercial 3.0 Unported Licence.

17 A. P. Mariano, M. J. Keshtkar, D. I. P. Atala, F. Maugeri Filho, M. R. Wolf Maciel, R. Maciel Filho and P. Stuart, *Energy Fuels*, 2011, **25**, 2347–2355.
18 I. Patraşcu, C. S. Bîldea and A. A. Kiss, *ACS Sustainable Chem. Eng.*, 2018, **6**, 5452–5461.
19 M. Matsumura, H. Kataoka, M. Sueki and K. Araki, *Bioprocess Eng.*, 1988, **3**, 93–100.
20 J. A. Gil, L. Túa, A. Rueda, B. Montaño, M. Rodríguez and D. Prats, *Desalination*, 2010, **250**, 997–1001.
21 C. Xue, X. Q. Zhao, C. G. Liu, L. J. Chen and F. W. Bai, *Biotechnol. Adv.*, 2013, **31**, 1575–1584.
22 G. Merlet, F. Uribe, C. Aravena, M. Rodríguez, R. Cabezas, E. Quijada-Maldonado and J. Romero, *J. Membr. Sci.*, 2017, **537**, 337–343.
23 R. Maurya, T. Ghosh, H. Saravaia, C. Paliwal, A. Ghosh and S. Mishra, *Bioresour. Technol.*, 2016, **221**, 251–261.
24 B. Bharathiraja, J. Jayamuthunagai, T. Sudharsanaa, A. Bharghavi, R. Praveenkumar, M. Chakravarthy and D. Yuvaraj, *Renewable Sustainable Energy Rev.*, 2017, **68**, 788–807.
25 N. Qureshi and I. S. Maddox, *Food Bioprod. Process.*, 2005, **83**, 43–52.
26 H. Gonzalez-Penas, T. A. Lu-Chau, M. T. Moreira and J. M. Lema, *Appl. Microbiol. Biotechnol.*, 2014, **98**, 5915–5924.
27 H. Bahrmann, H. D. Hahn and D. Mayer, *2-Ethylhexanol in Ullmann's Encyclopedia of Industrial Chemistry*, Wiley-VCH Verlag GmbH & Co. KGaA, Weinheim, 2000.
28 H. B. Park, C. H. Jung, Y. M. Lee, A. J. Hill, S. J. Pas, S. T. Mudie, E. Van Wagner, B. D. Freeman and D. J. Cookson, *Science*, 2007, **318**, 254–258.
29 J. H. Kim, S. H. Park, M. J. Lee, S. M. Lee, W. H. Lee, K. H. Lee, N. R. Kang, H. J. Jo, J. F. Kim, E. Drioli and Y. M. Lee, *Energy Environ. Sci.*, 2016, **9**, 878–884.
30 M. Cook, L. Peeva and A. Livingston, *Ind. Eng. Chem. Res.*, 2018, **57**, 730–739.
31 J. H. Kim, M. Cook, S. H. Park, S. J. Moon, J. F. Kim, A. G. Livingston and Y. M. Lee, *Green Chem.*, 2018, **20**, 1887–1898.
32 J. H. Kim, S. J. Moon, S. H. Park, M. Cook, A. G. Livingston and Y. M. Lee, *J. Membr. Sci.*, 2018, **550**, 322–331.
33 E. Elif Hamurcu and B. M. Baysal, *J. Polym. Sci. Pol. Phys.*, 1994, **32**, 591–594.
34 M. Hirose, T. Ohara and M. Ando, *US Pat.*, 5,733,602, 1998.
35 H. Fan, N. Wang, S. Ji, H. Yan and G. Zhang, *J. Mater. Chem. A*, 2014, **2**, 20947–20957.
36 S. Li, F. Qin, P. Qin, M. N. Karim and T. Tan, *Green Chem.*, 2013, **15**, 2180.
37 J. Huang, *J. Membr. Sci.*, 2001, **192**, 231–242.
38 A. G. Fadeev, Y. A. Selinskaya, S. S. Kelley, M. M. Meagher, E. G. Litvinova, V. S. Khotimsky and V. V. Volkov, *J. Membr. Sci.*, 2001, **186**, 205–217.
39 V. García, E. Pongrácz, E. Muurinen and R. L. Keiski, *Desalination*, 2009, **241**, 201–211.
40 S.-Y. Li, R. Srivastava and R. S. Parnas, *J. Membr. Sci.*, 2010, **363**, 287–294.
41 S. Liu, G. Liu, X. Zhao and W. Jin, *J. Membr. Sci.*, 2013, **446**, 181–188.
42 E. El-Zanati, E. Abdel-Hakim, O. El-Ardi and M. Fahmy, *J. Membr. Sci.*, 2006, **280**, 278–283.
43 Y. Li, J. Shen, K. Guan, G. Liu, H. Zhou and W. Jin, *J. Membr. Sci.*, 2016, **510**, 338–347.
44 Z. Zhang, D. Chen, Y. Chen, Y. Hao, M. O. Tade and Z. Shao, *J. Membr. Sci.*, 2014, **472**, 10–18.
45 S. D. Doig, A. T. Boam, A. G. Livingston and D. C. Stuckey, *J. Membr. Sci.*, 1999, **154**, 127–140.
46 P. R. Brookes and A. G. Livingston, *J. Membr. Sci.*, 1995, **104**, 119–137.
47 R. Valadezblanco, F. Ferreira, R. Jorge and A. Livingston, *J. Membr. Sci.*, 2008, **317**, 50–64.
48 Z. Jiang, S. Karan and A. G. Livingston, *Adv. Mater.*, 2018, **30**, e1705973.
49 S. J. Moon, J. H. Kim, J. G. Seong, W. H. Lee, S. H. Park, S. H. Noh, J. H. Kim and Y. M. Lee, *J. Membr. Sci.*, 2020, **607**, 118120.
50 A. P. Mariano, R. M. Filho and T. C. Ezeji, *Renewable Energy*, 2012, **47**, 183–187.
51 S. Sreekumar, Z. C. Baer, A. Pazhamalai, G. Gunbas, A. Grippo, H. W. Blanch, D. S. Clark and F. D. Toste, *Nat. Protoc.*, 2015, **10**, 528–537.
52 S. Chovau, S. Gaykawad, A. J. Straathof and B. Van der Bruggen, *Bioresour. Technol.*, 2011, **102**, 1669–1674.